JOURNAL OF THE
ELECTRON DEVICES SOCIETY

Received 7 December 2019; accepted 3 January 2020. Date of publication 15 January 2020; date of current version 27 January 2020.
The review of this paper was arranged by Editor M. Liu.

Digital Object Identifier 10.1109/JEDS.2020.2966799

Enhanced Switching Properties in TaO_x Memristors Using Diffusion Limiting Layer for Synaptic Learning

PEI-YU JUNG[1], DEBASHIS PANDA[2], SRIDHAR CHANDRASEKARAN[3], SAILESH RAJASEKARAN[4], AND TSEUNG-YUEN TSENG[1] (Fellow, IEEE)

1 Institute of Electronics, National Chiao Tung University, Hsinchu 30010, Taiwan
2 Department of Physics, National Institute of Science and Technology, Berhampur 761008, India
3 Department of EECS, National Chiao Tung University, Hsinchu 30010, Taiwan
4 Department of Materials Science and Engineering, National Chiao Tung University, Hsinchu 30010, Taiwan

CORRESPONDING AUTHOR: T.-Y. TSENG (e-mail: tseng@cc.nctu.edu.tw)

This work was supported in part by the Ministry of Science and Technology, Taiwan, under Project MOST 107-2221-E-009-089-MY3. The work of Debashis Panda was supported by the DST-SERB, Government of India under Grant SRG/2019/000129.

ABSTRACT To move towards a new generation powerful computing system, brain-inspired neuromorphic computing is expected to transform the architecture of the conventional computer, where memristors are considered to be potential solutions for synapses part. We propose and demonstrate a novel approach to achieve remarkable improvement of analog switching linearity in $TaN/Ta/TaO_x/Al_2O_3/Pt/Si$ memristors by varying Al_2O_3 layer thickness. Presence of the Al_2O_3 layer is confirmed from the Auger Electron Spectroscopy study. Good analog switching ratio of about 100× and superior switching uniformity are observed for the 1 nm Al_2O_3 based device. Multilevel capability of the memristive devices is also explored for prospective use as a synapse. More than 10^4 and 4×10^4 cycles nondegradable dc and ac endurances, respectively, alongwith 10^4 second retention are achieved for the optimized device. Improved linearities of 2.41 and −2.77 for potentiation and depression, respectively are obtained for such 1 nm Al_2O_3-based devices. The property of gradual resistance changed by pulse amplitudes confirms that the TaO_x memristors can be potentially used as an electronic synapse.

INDEX TERMS Memristors, synapse, neuromorphic computing.

I. INTRODUCTION

Recent days, novel computing architectures are proposed to solve the von Neumann bottleneck, where the physical separation between the data processing and the memory units in usual computers may increase limitations of latency and power consumption. Bio-inspired neuromorphic computing (NC) is expected to develop a more proficient computing architecture that mimics biological neural networks (NNs) [1]. Neurons and synapses are the two fundamental elements of neuromorphic architecture, where synapse plays an important role in learning and memory. Numerous studies are going on to implement the function of biological synapses into solid-state devices using emerging memories, where data are kept in the form of conductance [2]–[5]. Memristors [4], [6]–[8], [9], [10] are considered to be leading candidates, because memristor-based synapse [11]–[14] resembling biological synapse through complex ion-controlled mechanisms depends on neural signal strengths.

To implement the hardware NN (HNN), the key role is the effective design of a synaptic device, which is a combination of storage and computational capabilities. To build such neuromorphic systems two primary algorithms are considered: spike-timing-dependent-plasticity (STDP) [13] and back propagation (BP) [8], [11], [12], [15]. It is expected that the HNN synaptic devices based BP should have features such as small size, reliability, repeatability, low-power operation, linear and symmetric changes in conductance (equivalent to synaptic weight) with reference to the number of potentiation and depression pulses [11], [12], [16].

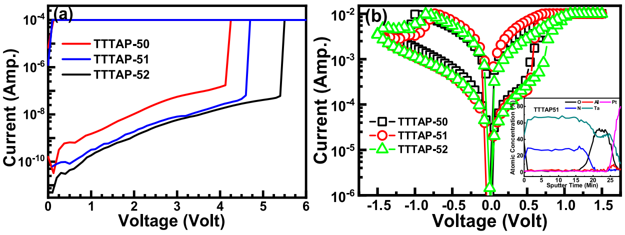

FIGURE 1. **(a) Forming voltage and (b) DC switching characteristics of TTTAP-50, TTTAP-51 and TTTAP-52 devices. Inset of (b) Typical auger depth profile spectra of TTTAP-51 device.**

In particular, memristors have low power consumption and exhibit excellent scalability (10 nm) in developing artificial synapses [17].

However, the major challenge of memristor-based neuromorphic system is to design a cell with faster operating speed, higher number of conductance states, lowest operation voltage, excellent retention, and comparable linearity for potentiation and depression. On the other hand, active layers of different binary oxides and metal electrodes as single or stack layers have been established for memristive devices. Therefore, optimization of the above parameters is a nontrifling concern in synaptic devices, an important area of research [17]. In this work, we investigated the engineering and optimization of the switching properties in TaO$_x$ based memristors by the insertion of a thin Al$_2$O$_3$ diffusion limiting layer (DLL). We reports the compositional properties, switching behaviour and synaptic characteristics of TaOx memristors with diffusion limiting layer.

II. EXPERIMENTS

A 70-nm thin Pt bottom electrode was deposited by e-beam evaporation on 30 nm thin Ti adhesion layer. A respective ultrathin Al$_2$O$_3$ layer with different thicknesses (β nm; $\beta = 0, 1,$ and 2 nm) was deposited by atomic layer deposition (ALD) at 250°C using the precursor trimethyle aluminium, $(CH_3)_3Al$, so-called TMA. An optimized 25 nm TaO$_x$ was deposited on it using reactive DC sputtering at 300 W from Ta target. To achieve best pulse synaptic properties, we have deposited 5 nm thin Ta intermediate layer by DC sputters at pure Ar ambient. Finally, a 50 nm thin TaN top electrode (TE) (diameter of 150 μm) was DC sputtered using a shadow mask. The various samples are named as TTTAP-50, TTTAP-51, and TTTAP-52 for the structure TaN/Ta (5 nm)/TaO$_x$ (25 nm)/Al$_2$O$_3$ (β nm)/Pt having different Al$_2$O$_3$ layer with β varied from 0, 1, and 2 nm, respectively. The film compositions at different depth were studied using Auger Electron Spectroscopy (AES) (VG Scientific Microlab 310F). Different electrical switching characteristics were measured using Agilent B1500A and an Agilent B1530A arbitrary waveform generator fast measurement unit by applying all voltage signal on the TaN TE while keeping the Pt bottom electrode (BE) grounded.

III. RESULTS AND DISCUSSION

Forming is necessary for all the devices to initiate the switching process by applying a positive voltage of 6 V across the devices, as shown in Fig. 1(a). A relatively higher forming voltage after insertion of 1 and 2 nm Al$_2$O$_3$ layers compared to the devices without Al$_2$O$_3$ layer having same TaO$_x$ thickness is attributed to the highly insulating nature of Al$_2$O$_3$ along with an increase in total thickness. Bipolar switching characteristics of all the TTTAP devices are depicted in Fig. 1(b). During the positive voltage ramp, the device's resistance is changed from the high resistance state (HRS) to low resistance state (LRS), while during the negative bias ramp, it is changed from LRS to HRS. The device returns to HRS again at −1, −0.73, and −0.85 V for TTTAP-50, TTTAP-51, and TTTAP-52 devices, respectively. The initial resistance is decreased to about 2.8 kΩ during the set process for all the devices, as compared to that of the device without forming, indicating the partial rupture of filaments during the first reset after forming.

About 30X switching window is observed for all the devices, indicating the device can also be used for multi-level cell (MLC) applications. For analog switching application, the reset process always exhibits gradual changes in current. The Gibbs free energies of the oxidation states of Al$_2$O$_3$and TaO$_x$ are −1582.9 and −764.4 kJ/mol, respectively [18]. Moreover, compared with the sputtered TaO$_x$, the Al$_2$O$_3$ layer grown by ALD seems to have a denser microstructure due to the fabrication process. The higher amount of oxygen vacancies in TaO$_x$ contributes to impede ion diffusion. Since, Al$_2$O$_3$has lower Gibbs free energy, good stability and lower ion diffusion speed [19], it can limit the ion diffusion speed and also confine the path of the filament. As a result, the gradual switching is observed under DC voltage sweeps in the memristors having 2 nm Al$_2$O$_3$ layer, as shown in Fig. 1(b). The presence of Al$_2$O$_3$ layer is confirmed from the signal of Al in the AES spectra as shown in the inset of Fig. 1(b). No metal/ semiconductor impurities such as Ta, Al and Pt atoms diffused into TaO$_x$ are observed.

The multi-level characteristic of the TTTAP-51 devices is illustrated in Fig. 2(a) by controlling the set compliance and also reset stop voltages. The ion movement and redox reaction were recognized as two of the most important parameters that determine the dynamics of filament growth and dissolution in filamentary RRAM [20]. To imitate the functions of a biological synapse we have studied an analog memory having multiple states in between the HRS and LRS. As shown in Fig. 2(a) the sweep sequence of 1 to 10 is achieved by getting continuous set (potentiation) by the variation of repeated increase of set compliance from 500 μA to 10 mA with 1.5 V set voltage, fixed −1.8 V reset voltage and the gradual decreases of the resistance from HRS to LRS. Finally, a continuous reset (depression) is performed by the successive increase of the reset stop voltage from −1.2 to −2.2 V with the constant set voltage of 1.5V with 10mA compliance current. Hence, the device's resistance progressively increases from LRS to HRS. The resistances are continuously varied, and multiple resistance states are

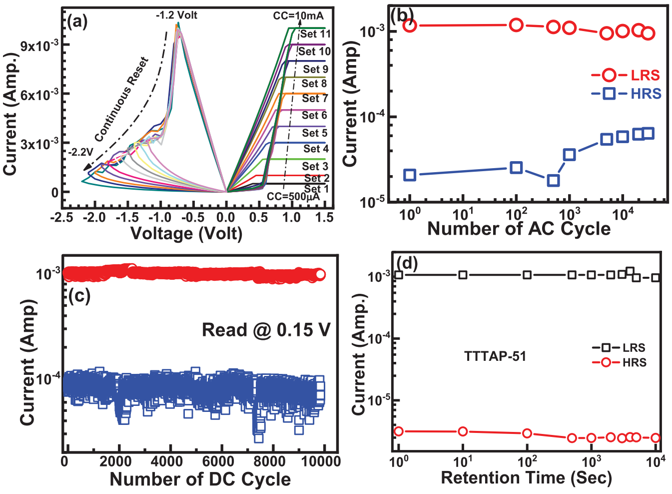

FIGURE 2. **(a) MLC, (b) and (c) pulse and DC endurance respectively and (d) retention characteristics of TTTAP-51 device. (Transient pulses used, set: 2V/100 ns and reset: −1.8 V/100 ns).**

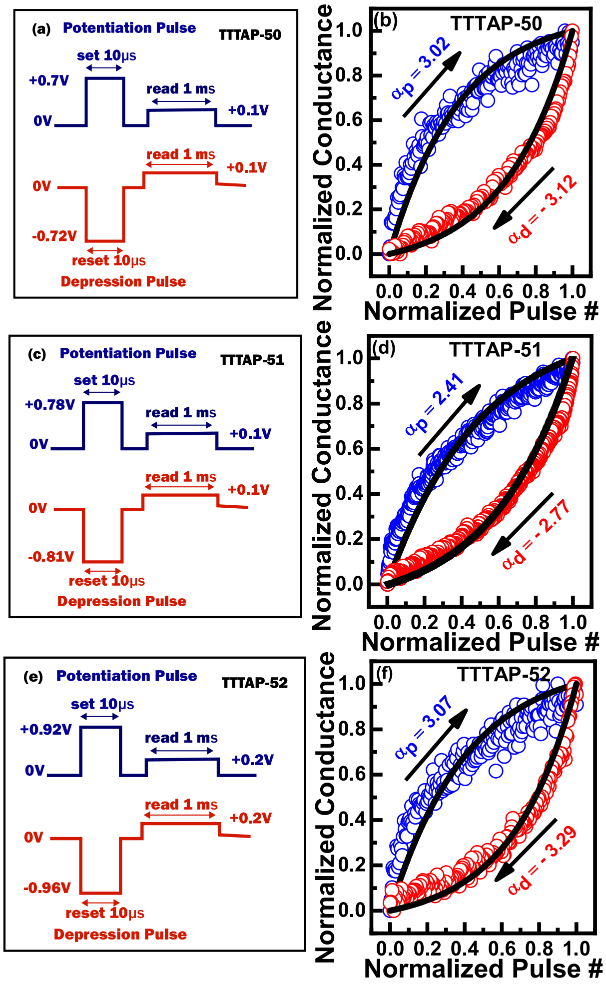

FIGURE 3. **(a) (c) and (e) Pulse scheme and (b), (d) and (f) normalized conductance state distribution for potentiation and depression along with the fitting curve of TTTAP-50, TTTAP-51 and TTTAP-52 devices respectively.**

achieved. This gradual set process is due to the formation of stronger conducting filaments (CFs) having larger diameters or multiple CFs produced with higher current through the oxide matrix [21]. However, partial annihilation of CFs with a longer ruptured length can be responsible for such gradual reset [22].

The AC endurance of TTTAP-51 device was studied and the result is shown in Fig. 2(b) indicating the pulse cycling for more than 3×10^4 cycles. A transient 1.8 V set and −2 V reset pulse with 100 ns width was applied to switch the device between HRS and LRS. The current was read out by a 0.1 V voltage at each sampling point. It is shown in Fig. 2(b) that the HRS resistance finally tends to decrease because the unrecoverable oxygen vacancies in the oxide matrix accumulate from cycle to cycle. However, the resistance window is still very large for more than 3×10^4 cycles. Especially, the result shows that the device has a fast switching speed of less than 100 ns. The DC endurance characteristics are also investigated. More fluctuations are found in HRS for the TTTAP-50 compared to TTTAP-51 and TTTAP-52 devices (Data not shown). As seen from Fig. 2(c), DC endurance of more than 10^4 cycles is observed for TTTAP-51 device. LRS and HRS are found to be stable with a ratio of around 10^2 order. The optimized device also exhibits excellent retention of 10^4 s, as shown in Fig. 2(d).

For the practical application of electronic synaptic devices, the devices need to be worked under the pulse input signal rather than the dc voltage ramp. Hence, the property of gradual resistance change with the pulse cycling was investigated. Linearity and stability (cycle-to-cycle) of synaptic weight update of consecutive potentiation and depression, which are two critical parameters for the synaptic devices. To improve the linearity and switching stability of potentiation and depression, the effect of insertion of the Al_2O_3 on the Pt/TaO$_x$ interface was studied, shown in Fig. 3. To achieve best pulse cycling slightly different pulse amplitude (optimized) is applied during training for the different devices. An identical pulse of 0.7 V amplitude and 10 μs width and −0.72 V amplitude and 10 μs width for the potentiation and depression pulse train were applied, respectively. The 1 ms pulse width and 0.1V amplitude reading are used for both the potentiation and depression in TTTAP-50 devices, as shown in Fig. 3(a). However, for the TTTAP-51 devices, a pulse of 0.78 V amplitude and 10 μs width and −0.81 V amplitude and 10 μs width for the potentiation and depression pulse train were applied, respectively, as shown in Fig. 3(c). In case of TTTAP-52 devices, a pulse of 0.92 V amplitude and 10 μs width and −0.96 V amplitude and 10 μs width for the potentiation and depression pulse train were applied, respectively, as shown in Fig. 3(e). Pulse parameters for both the potentiation and depression were finely tuned in each cases to achieve the best switching linearity for fair comparison.

Fig. 3(b), Fig. 3(d), and Fig. 3(f), represents the potentiation and depression curve of TTTAP-50, TTTAP-51, and TTTAP-52 devices of a cycle with the MATLAB simulated

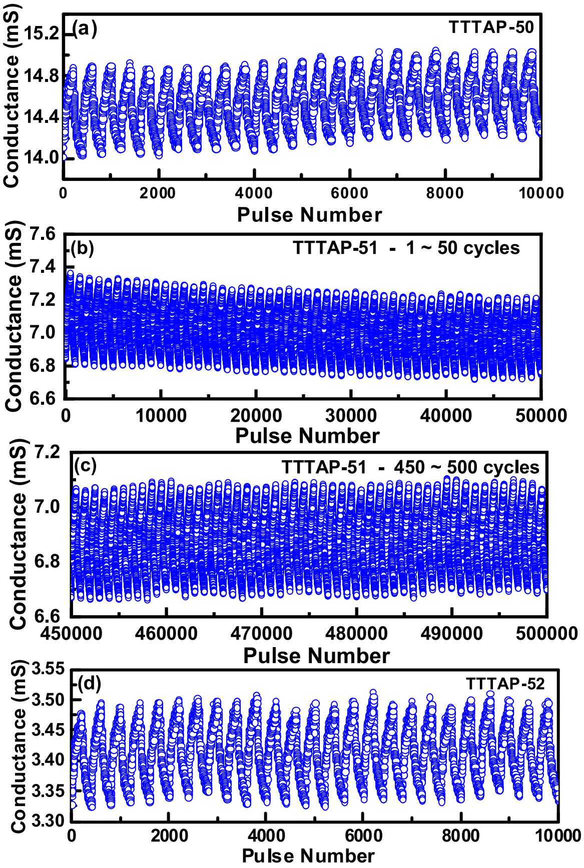

FIGURE 4. Cyclic repetition of epoch of (a) TTTAP-50, (b) 1st to 50th cycles of TTTAP-51, (c) last 450th to 500th cycle with a total of 500000 training pulses of TTTAP-51 and (d) TTTAP-52 devices.

curve to find nonlinearity value [23]. As shown in the figure, the nonlinearities of the TTTAP-51 devices are improved to 2.41 and −2.77 for potentiation and depression, respectively. A synaptic characteristic with only 25 cycles having small degradation are observed for the TTTAP-50 and TTTAP-52 devices, as shown in Figs. 4(a) and (d). However, Figs. 4(b) and (c) indicate that the TTTAP-51 device can survive more than 500 cycles of potentiation and depression. Fig. 4(b) shows the first 50 cycles; and Fig. 4(c) shows the last 450th to 500th cycle, indicating excellent reproducible synaptic characteristics of more than 500 times with little conductance drifting. However, the small variation of conductance by approximately 4% can be explained as the semiconducting like transport phenomenon such as Schottky, Pool-Frenkel, Fowler–Nordheim etc. of the oxide films.

Table 1, shows the comparison of different important parameters like conductance states, nonlinearity, pulse condition, potentiation and depression (P/D) cycles. our work is comparable with the other works, having higher conductance states, lowest operation voltage and faster operating speed. Moreover, other works almost didn't discuss about their device stability, our device can repeat 500 P/D cycles and DC endurance can reach more than 10^4 cycles. The comparison of potentiation and depression nonlinearity with the literature is summarized in Fig. 5. Therefore, it's obvious that after the insertion of ultra-thin Al_2O_3 film, the device can improve not only the conductance modulation linearity but also show the superior reproducible synaptic characteristics. This synaptic RRAM is one of the potential candidates for the next generation neuronal circuits.

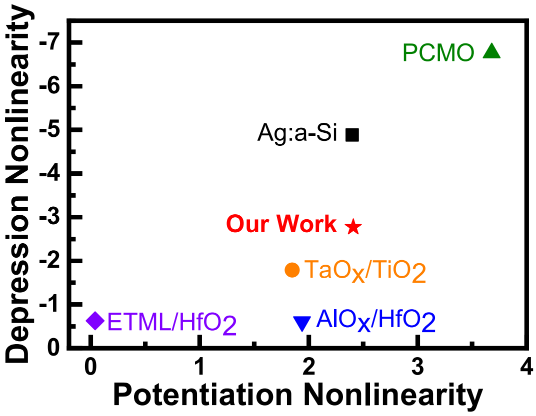

FIGURE 5. Comparison of potentiation and depression nonlinearity with the value obtained from literature.

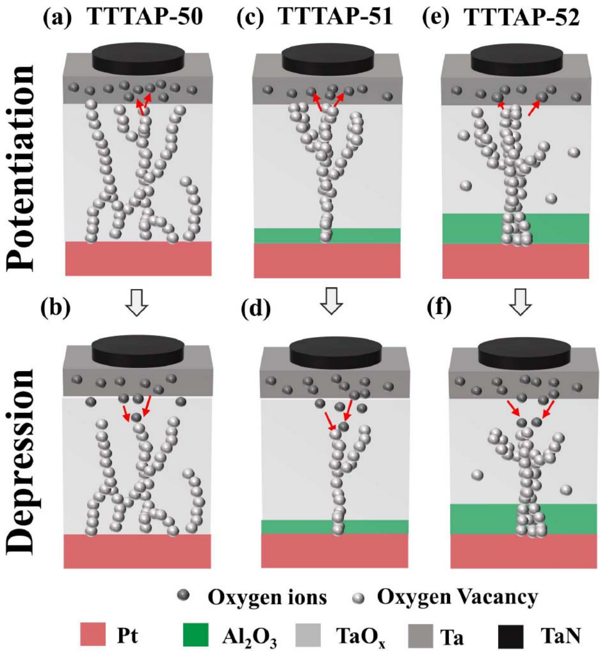

FIGURE 6. Schematic conduction mechanism for potentiation and depression of the devices (a, b) TTTAP-50, (c, d) TTTAP-51 and (e, f) (a, b) TTTAP-52 devices respectively.

The switching mechanism of TaOx-based RRAM is commonly understood as the field dependent oxygen vacancy migration from/ to a source layer thereby forming/ rupturing the filament based on oxygen vacancy by redox reaction [24]. Fig. 6(a and b) is a schematic illustration of switching processes for TaN/Ta/TaO_x/Pt device. During forming, soft dielectric breakdown occurs and oxygen ions drift to the anode interface by the high electric field. Due

TABLE 1. Summary of Al_2O_3 doped TaO_x memristors key metrics for neuromorphic computing and comparison with other technologies surveyed in references [22]–[27].

Type of RRAM	**Ag:a-Si [22]**	**TaOx/ TiO_2 [23]**	**PCMO [24]**	**AlOx/ HfO_2 [25]**	**ETML/H fO_2 [26]**	**ECRAM [27]**	**Our Work**
# of conductance states	97	102	50	40	120	55	**500**
Nonlinearity (weight increase/ decrease)	2.40/ -4.88	1.85/ -1.79	3.68/ -6.76	1.94/ -0.61	0.04/-0.63	0.347 / 0.268	**2.41/ -2.77**
Weight increase pulse	3.2V/ 300µs	3V/ 40ms	-2V/1ms	0.9V/ 100µs	1.6V/ 50ns	I_G = 100 pA and pulse width = 1 s	**0.78V/ 10µs**
Weight decrease pulse	-2.8V/ 300µs	-3V/ 10ms	2V/1ms	-1V/ 100µS	1.5V/ 50ns	I_G = -100 pA and pulse width = 1 s	**-0.81V/ 10µs**
Repeated P/D cycles	--	50	--	3	1000	50	**500**

to the oxygen-gettering ability [25] of Ta layer, it behaves like an oxygen reservoir, and the constriction part of the filament was located at the Ta/TaO_x interface. Since we have observed some fluctuations of current in HRS in Fig. 2(b), we consider it may be due to the formation of multi-branch filament [26]. This multiple filament type analog RRAM has medium oxygen vacancy concentration and relatively wider conductive filament region, which is good for linear analog switching [27]. On applying the repeated pulse numbers, the oxygen ion motion assists the formation of oxygen vacancy based conducting filament and Ta layer traps the oxygen ions during potentiation operation. Conversely, on introducing negative pulse numbers, the trapped oxygen ions in the Ta layer undergo electrochemical interaction and reduce the oxygen vacancy-based filament.

Fig. 6(c-e) shows the schematic of switching processes for $TaN/Ta/TaO_x/Al_2O_3/Pt$ device. Since Al_2O_3has lower Gibbs free energy, once the filament forms, it will be confined along the same path, significantly affecting the growth of the filament to be single and thinner near the bottom electrode while maintaining multi-branch type filament near the top electrode [28], [29]. Therefore, with Al_2O_3, the device having stable conducting filament growth which directly leads to higher repeatable and reliable switching performance but also maintaining the high conductance tuning linearity as observed in Fig. 4(c).

IV. CONCLUSION

In conclusion, $TaN/Ta/TaO_x/Al_2O_3/Pt$ memristors by changing the thickness of Al_2O_3 layer from 0 to 2 nm is fabricated. AES spectra confirmed the presence of Al_2O_3 layer in the device. A good analog switching of about 100× and excellent device uniformity are observed for the devices having 1 nm Al_2O_3 layer. The MLC applications and long retention of 10^4 seconds are also observed for the optimized devices. The same device is also sustained more than 10^4 cycles dc and 4×10^4 cycles ac endurance. The linearity of the 1 nm Al_2O_3 layer-based device is improved to 2.41 and -2.77 for potentiation and depression respectively. Improved synaptic linearity of this memristive devices indicates the device can be potentially used for the emerging neuromorphic computing devices as an electronic synapse.

REFERENCES

[1] C. Mead, "Neuromorphic electronic systems," *Proc. IEEE*, vol. 78, no. 10, pp. 1629–1636, Oct. 1990.
[2] S. Chandrasekaran, F. M. Simanjuntak, T.-L. Tsai, C.-A. Lin, and T.-Y. Tseng, "Effect of barrier layer on switching polarity of ZrO_2-based conducting-bridge random access memory," *Appl. Phys. Lett.*, vol. 111, no. 11, Sep. 2017, Art. no. 113108.
[3] S. Chandrasekaran, F. M. Simanjuntak, R. Saminathan, D. Panda, and T.-Y. Tseng, "Improving linearity by introducing Al in HfO_2 as memristor synapse device," *Nanotechnology*, vol. 30, no. 44, 2019, Art. no. 445205.
[4] D. Panda and T.-Y. Tseng, "Growth, dielectric properties, and memory device applications of ZrO_2 thin films," *Thin Solid Films*, vol. 531, pp. 1–20, Mar. 2013.
[5] Y. Kaneko, Y. Nishitani, and M. Ueda, "Ferroelectric artificial synapses for recognition of a multishaded image," *IEEE Trans. Electron Devices*, vol. 61, no. 8, pp. 2827–2833, Aug. 2014.
[6] D. Panda and T.-Y. Tseng, "One-dimensional ZnO nanostructures: Fabrication, optoelectronic properties, and device applications," *J. Mater. Sci.*, vol. 48, no. 20, pp. 6849–6877, Oct. 2013.
[7] D. Panda, C.-Y. Huang, and T.-Y. Tseng, "Resistive switching characteristics of nickel silicide layer embedded HfO_2 film," *Appl. Phys. Lett.*, vol. 100, no. 11, 2012, Art. no. 112901.
[8] M. Prezioso, F. Merrikh-Bayat, B. D. Hoskins, G. C. Adam, K. K. Likharev, and D. B. Strukov, "Training and operation of an integrated neuromorphic network based on metal-oxide memristors," *Nature*, vol. 521, no. 7550, pp. 61–64, May 2015.

[9] A. Prakash, D. Jana, and S. Maikap, “TaO_x-based resistive switching memories: Prospective and challenges,” *Nanoscale Res. Lett.*, vol. 8, no. 1, p. 418, 2013.
[10] S. Samanta *et al.*, “Understanding of multi-level resistive switching mechanism in GeO_x through redox reaction in H_2O_2/sarcosine prostate cancer biomarker detection,” *Sci. Rep.*, vol. 7, no. 1, pp. 1–12, 2017.
[11] I.-T. Wang, C.-C. Chang, L.-W. Chiu, T. Chou, and T.-H. Hou, “3D Ta/TaO_x/TiO_2/Ti synaptic array and linearity tuning of weight update for hardware neural network applications,” *Nanotechnology*, vol. 27, no. 36, Sep. 2016, Art. no. 365204.
[12] G. Bi and M. Poo, “Synaptic modifications in cultured hippocampal neurons: Dependence on spike timing, synaptic strength, and postsynaptic cell type,” *J. Neurosci.*, vol. 18, no. 24, pp. 10464–10472, Dec. 1998.
[13] S. Yu, B. Gao, Z. Fang, H. Yu, J. Kang, and H.-S. P. Wong, “A neuromorphic visual system using RRAM synaptic devices with Sub-pJ energy and tolerance to variability: Experimental characterization and large-scale modeling,” in *Proc. Int. Electron Devices Meeting*, 2012, pp. 1–4.
[14] M. Suri *et al.*, “CBRAM devices as binary synapses for low-power stochastic neuromorphic systems: Auditory (cochlea) and visual (retina) cognitive processing applications,” in *Proc. Int. Electron Devices Meeting*, 2012, pp. 1–4.
[15] D. Kuzum, S. Yu, and H. S. Philip Wong, “Synaptic electronics: Materials, devices and applications,” *Nanotechnology*, vol. 24, no. 38, 2013, Art. no. 382001.
[16] G. W. Burr *et al.*, “Experimental demonstration and tolerancing of a large-scale neural network (165 000 synapses) using phase-change memory as the synaptic weight element,” *IEEE Trans. Electron Devices*, vol. 62, no. 11, pp. 3498–3507, Nov. 2015.
[17] Y. Jeong, S. Kim, and W. D. Lu, “Utilizing multiple state variables to improve the dynamic range of analog switching in a memristor,” *Appl. Phys. Lett.*, vol. 107, no. 17, Oct. 2015, Art. no. 173105.
[18] J.-S. Huang, S. Kim, and W. D. Lu, “Bias polarity-induced transformation of point contact resistive switching memory from single transparent conductive metal oxide layer,” *Adv. Electron. Mater.*, vol. 1, no. 8, Aug. 2015, Art. no. 1500061.
[19] R. Nakamura *et al.*, “Diffusion of oxygen in amorphous Al_2O_3, Ta_2O_5, and Nb_2O_5,” *J. Appl. Phys.*, vol. 116, no. 3, Jul. 2014, Art. no. 033504.
[20] Z. Wang *et al.*, “Engineering incremental resistive switching in TaO_X based memristors for brain-inspired computing,” *Nanoscale*, vol. 8, no. 29, pp. 14015–14022, 2016.
[21] L. Goux *et al.*, “On the gradual unipolar and bipolar resistive switching of TiN\HfO_2\Pt memory systems,” *Electrochem. Solid-State Lett.*, vol. 13, no. 6, pp. 54–56, 2010.
[22] M. J. Rozenberg, M. J. Sánchez, R. Weht, C. Acha, F. Gomez-Marlasca, and P. Levy, “Mechanism for bipolar resistive switching in transition-metal oxides,” *Phys. Rev. B, Condens. Matter*, vol. 81, no. 11, Mar. 2010, Art. no. 115101.
[23] W. Wu *et al.*, “A methodology to improve linearity of analog RRAM for neuromorphic computing,” in *Dig. Tech. Paper IEEE Symp. VLSI Technol.*, Jun. 2018, pp. 103–104.
[24] J. J. Yang *et al.*, “High switching endurance in TaO_x memristive devices,” *Appl. Phys. Lett.*, vol. 97, no. 23, Dec. 2010, Art. no. 232102.
[25] Z. Wei *et al.*, “Highly reliable TaOx ReRAM and direct evidence of redox reaction mechanism,” in *Proc. IEEE Int. Electron Devices Meeting*, 2008, pp. 1–4.
[26] V. R. Nallagatla, J. Jo, S. K. Acharya, M. Kim, and C. U. Jung, “Confining vertical conducting filament for reliable resistive switching by using a Au-probe tip as the top electrode for epitaxial brownmillerite oxide memristive device,” *Sci. Rep.*, vol. 9, no. 1, p. 1188, Dec. 2019.
[27] B. Gao *et al.*, “Modeling disorder effect of the oxygen vacancy distribution in filamentary analog RRAM for neuromorphic computing,” in *Proc. IEEE Int. Electron Devices Meeting (IEDM)*, 2017, pp. 1–4.
[28] L. Zhang *et al.*, “Unipolar TaO_x-based resistive change memory realized with electrode engineering,” *IEEE Electron Device Lett.*, vol. 31, no. 9, pp. 966–968, Sep. 2010.
[29] W. Banerjee, X. Xu, H. Lv, Q. Liu, S. Long, and M. Liu, “Variability improvement of TiO_x/Al_2O_3 bilayer nonvolatile resistive switching devices by interfacial band engineering with an ultrathin Al_2O_3 dielectric material,” *ACS Omega*, vol. 2, no. 10, pp. 6888–6895, Oct. 2017.

PEI-YU JUNG received the M.S. degree in electrical engineering from National Chiao Tung University, Hsinchu, Taiwan, in 2019. She is currently an Research and Development Engineer with TSMC, Hsinchu, Taiwan. Her research focuses in RRAM based synapse devices for neuromorphic systems.

DEBASHIS PANDA received the Ph.D. degree from IIT Kharagpur. He served as Postdoctoral Fellow with NCTU, Taiwan; University of Utah, USA; and NUS, Singapore. He is currently serving as an Associate Professor and the Head of the Department of Physics with the National Institute of Science and Technology, India. He awarded Indian Academies Summer Research Fellowship 2016, and also INSA Visiting Scientist in 2017. He also serves as a Visiting Scientist with NCTU, Taiwan; NPL, New Delhi; and IIT Kharagpur. His present research interest includes the design and fabrication of low power, highly reliable transparent flexible wearable artificial inorganic/organic synapse memristors for neuromorphic computing. He is a fellow of Indian Physical Society.

SRIDHAR CHANDRASEKARAN received the M.Tech. degree in VLSI design from SRM University, Chennai, India, in 2014, and the Ph.D. degree in electrical engineering and computer science from National Chiao Tung University, Hsinchu, Taiwan.

His research interest includes resistive synapse for artificial neural networks. He was awarded for outstanding academic research performance in 2017, through CTCI foundation.

SAILESH RAJASEKARAN received the M.S. degree in nanoscience and nanotechnology from SRM University, Chennai, India, in 2013. He is currently pursuing the Ph.D. degree in material sciences and engineering from National Chiao Tung University, Taiwan. His research focuses primarily on a highly-flexible and transparent wearable synapse memristor for neuromorphic computing and ultraviolet light exposure-based CBRAM.

TSEUNG-YUEN TSENG (Fellow, IEEE) was the Dean of the College of Engineering and the Vice Chancellor of the National Taipei University of Technology, Taiwan. He is currently a Lifetime Chair Professor with the Institute of Electronics, National Chiao Tung University, Taiwan. He was a recipient of the Distinguished Research Award from the Ministry of Science and Technology, the Academic Award and the National Endowed Chair Professor of Ministry of Education, the IEEE CPMT Outstanding Sustained Technical Contribution Award, and the Exceptional Technical Achievement Award.